LA-UR-83-2364

LA-UR--83-2364

DE83 017322

Los Alamos National Laboratory is operated by the University of California for the United States Department of Energy under contract W-7405-ENG-36.

TITLE: THERMAL DESIGN FOR PROTECTION OF DOWNHOLE ELECTRONIC PACKAGES

AUTHOR(S): Gloria A. Bennett
Gail R. Sherman

SUBMITTED TO: The 1983 Winter Annual Meeting of the American Society of Mechanical Engineers/Heat Transfer Division to be held November 13-18. 1983 in Boston. MA.

Los Alamos National Laboratory
Los Alamos, New Mexico 87545

FORM NO. 836 R4
ST. NO. 2629 5/81

DISCLAIMER

THERMAL DESIGN FOR PROTECTION OF DOWNHOLE ELECTRONIC PACKAGES

Gloria A. Bennett and Gail R. Sherman
Los Alamos National Laboratory
Los Alamos, NM 87545

ABSTRACT

This report describes design improvements made for downhole tools based on results obtained from the thermal analysis of the instrument package. Results include heat flux at the tool surface and temperature-time histories of each subsystem.

The research stems from a need for tools that can survive the harsh environment present in geothermal wellbores. The high temperatures and pressures create stress on the tools that function in this environment. Improvements in the design of downhole tools lead to more accurate data obtained from the wellbore during experimentation.

The analysis showed that the thermal potential and the conductance between electronics and its heat sink was too small and was misdirected. Significant improvements were achieved by increasing the available thermal capacity of the heat sink, the thermal potential between the heat sink and electronics, and the conductance of the heat transfer paths.

NONEMCLATURE

A = area
c_p = specific heat at constant pressure
h^p = convective film coefficient
K = thermal conductivity
Q = heat
T = temperature
r = radial coordinate
V = tool velocity
z = axial coordinate
Δ = change in
τ - time
ρ = density

Subscripts

c = convective
o = initial
p = pressure
∞ = ambient

INTRODUCTION

The goal of the Hot Dry Rock (HDR) Program is to investigate the feasibility of extracting thermal energy from naturally hot, but essentially dry formations, by circulating water from an injection well through artificially made hydraulic fractures to a production well drilled nearby (Fig. 1). Successful development of energy extraction techniques requires extensive data about water chemistry, acoustic signals, temperature, temperature changes, pressure, and flow rates at various depths in and between the two wells. The tools and downhole electronics used in making these physical measurements must withstand the heat and severe wellbore conditions to which they are repeatedly subjected. The purpose of this investigation is to improve the design of downhole tools so that they can withstand the harsh environment and furnish the accurate and extensive data required to achieve the goals of the Hot Dry Rock Program. The design improvements are based on four finite element analyses that have been completed for an acoustical tool with a typical thermal protection system. The model is a lumped mass approximation of the real components in each section of the tool. The analyses define thermal conditions, heat fluxes, and boundary and temperature conditions which vary as functions of time and temperature.

BACKGROUND

The two wellbores at the Fenton Hill site (FHS) that are being used to develop a commercial size reservoir are about 4600 m deep have a bottom-hole temperature of 593 K and a hydrostatic pressure of 40.3 E+06 Pa. The bottom 1200 m of each wellbore is open hole and is inclined at 35° to the vertical (1). Because of substances introduced during the drilling process, water chemistry in the FHS wells can vary between neutral, pH=7 to very basic, pH=11. Such conditions require downhole electronic tools to be packaged in a pressure vessel that can withstand abrasion, corrosion, high temperature and high pressure.

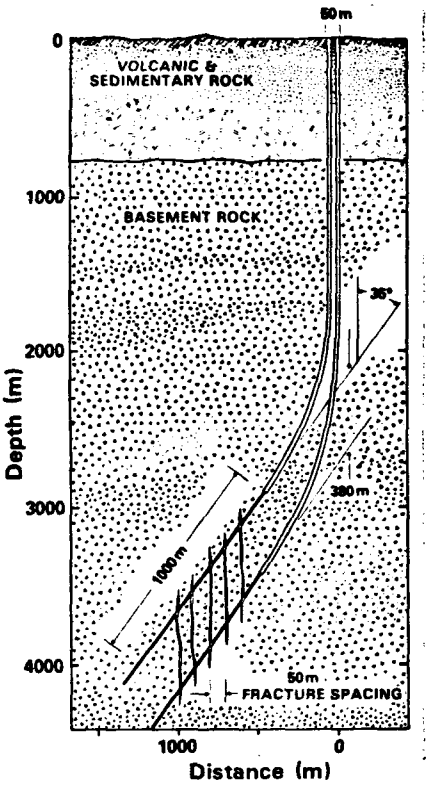

Fig. 1. Fenton Hill site geothermal wells.

Previously, tools and electronics had survived the conditions in a FHS demonstration reservoir (2) which was 2930 m deep and 470 K, but exposure to the higher temperatures and heat fluxes in the deeper wells caused thermal failure. Problems arise when measurements must be made at temperatures above the upper limit of 480 K (3), which occurs at FHS well depths below 3000 m.

The original thermal protection design places the electronics and a heat sink inside a tall, slender dewar that protects the package from radiation heat transfer. A cut-away illustration is shown in Fig. 2. The sensors, batteries, circuit boards, and other components are mounted on brass rods held in place by copper bulkheads. Power dissipation from the electronics is approximately 1 watt and is considered negligible compared to the heat entering the tool from a hot geothermal wellbore. While parked on station the tool is subjected to a high heat flux (shown in Fig. 10) at 502 K. The heat that enters the electronics from the wellbore must be transferred to the heat sink. The heat sink is tightly attached to the bulkhead nearest the open end of the dewar. The rods and bulkheads are the only high-conductance heat transfer paths from the electronics to the heat sink. The heat sink, filled with Woods Metal, is intended to absorb heat from the electronics, melting the Woods Metal at a temperature below the maximum temperature at which electronic components can be reliably exposed. Figure 3 illustrates the temperature history expected during operation and Fig. 4 shows the results of the downhole test. The temperature sensor mounted in the electronics section was expected to show a temperature increase up to the Woods Metal melting point, then a constant temperature while the absorbed heat melted the Woods Metal, and finally another temperature increase after all the heat sink is completely melted. Instead, the temperature history showed a steadily climbing

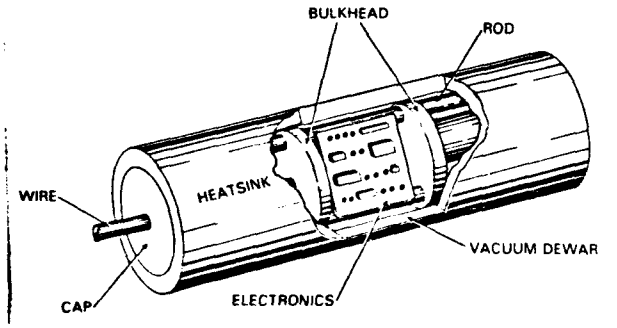

Fig. 2. Thermal protection system components.

temperature with no levelling at the Woods Metal melting point.

There are numerous possible explanations for the observed temperature history: (a) the sensor failed or was inaccurate, (b) the heat sink was already melted, (c) the air temperature was actually higher than the heat sink temperature, or (d) the heat transfer paths available for moving heat from electronics to heat sink were physically too small or their conductance was too small, and (e) the thermal potential between electronics and heat sink was too small or was in the wrong direction. This instrument was tested at 3340-m depth where the temperature is 493 K. It failed thermally after 2-1/3 h. This amount of time allows a single trip into and out of the FHS wells. In order to provide effective and sufficient measurements of geophysical data, the tool must have a thermal lifetime of at least 10 hours.

Examination of the system immediately following the test showed that the heat sink material was still solid and the sensor was found to be operational and accurate. The other explanations both involve determining the temperature of each subsystem. This determination requires either a detailed thermal analysis or extensive instrumentation and testing.

THERMAL ANALYSIS

Four thermal analyses were made of the instrument section of the tool. Numerical calculations were made using the AYER (4) finite element heat conduction code, which solves the generalized two-dimensional heat conduction equation implicitly. Meshes of the models were constructed using ZONE (5), a linear finite element

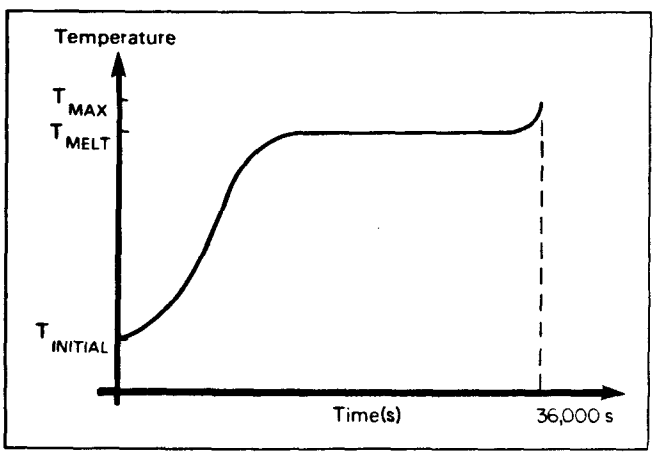

Fig. 3. Expected temperature history.

mesher and input data was prepared using a preprocessor program. A postprocessor program was used to plot the results, which are presented in the form of temperature histories, heat flux histories, and plots of temperature versus position.

The right hand side of the axisymmetric geometry is shown in Fig. 5. It assumes that there are no material or geometric variations in the θ-direction, which is strictly true only for the heat-sink section shown in Fig. 6. The battery and electronics sections, Figs. 7 and 8, have symmetry in approximately 180° angular segments and were modeled as lumped masses with equivalent smeared thermal properties of the copper, steel, and phenolic components. The heat sink is a lumped mass containing steel and Woods Metal.

The material property equations used throughout the analysis are given in Reference 6. Each equation was obtained by least squares regression on the data.

The partial differential equations of interest are given in Reference 7.

$$\frac{\partial T}{\partial \theta^2} = \frac{K}{\rho c_p}\left[\frac{\partial^2 T}{\partial x^2} + \frac{\partial^2 T}{\partial y^2}\right] \text{ and} \qquad (1)$$

$$\frac{\partial T}{\partial \theta} = \frac{K}{\rho c_p}\left[\frac{1}{r}\frac{\partial T}{\partial r} + \frac{\partial^2 T}{\partial r^2} + \frac{\partial^2 T}{\partial z^2}\right]. \qquad (2)$$

They are solved numerically using the finite element formulation and an implicit solution technique. These equations are second-order in two independent space variables and time and are quasi-linear because the material properties are allowed to vary with

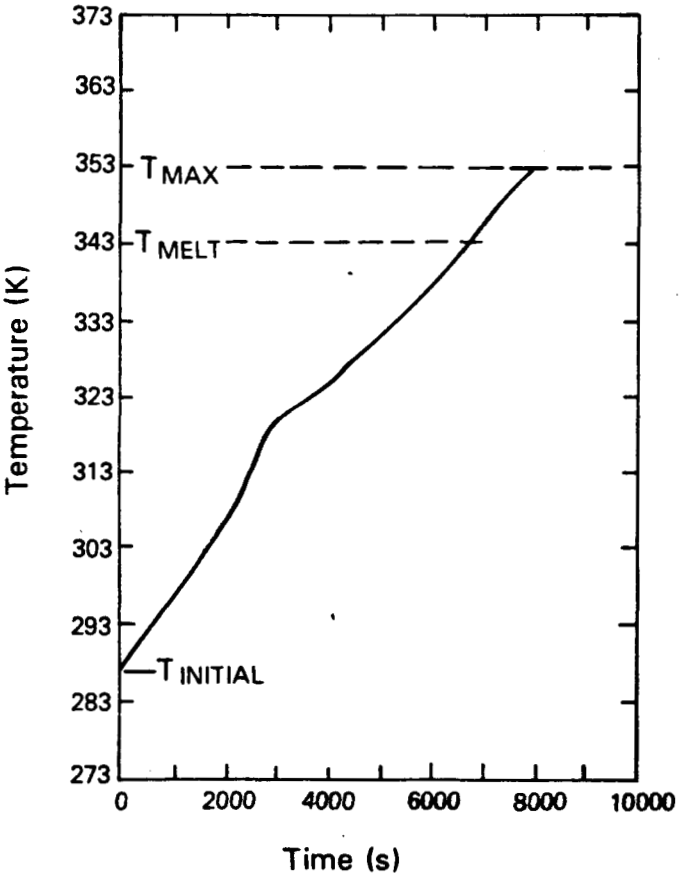

Fig. 4. Instrument test temperature history.

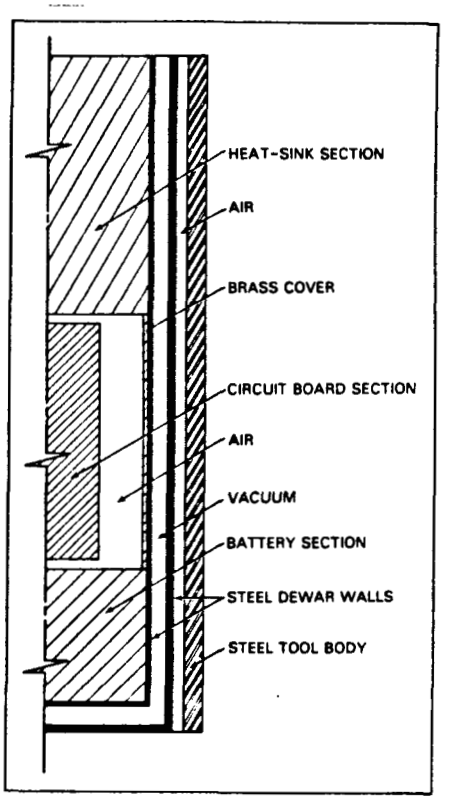

Fig. 5. Right hand side of axisymmetric model.

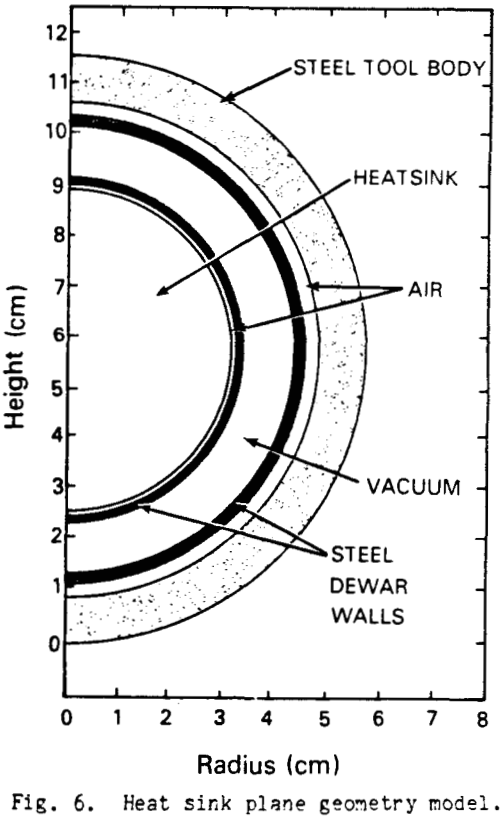

Fig. 6. Heat sink plane geometry model.

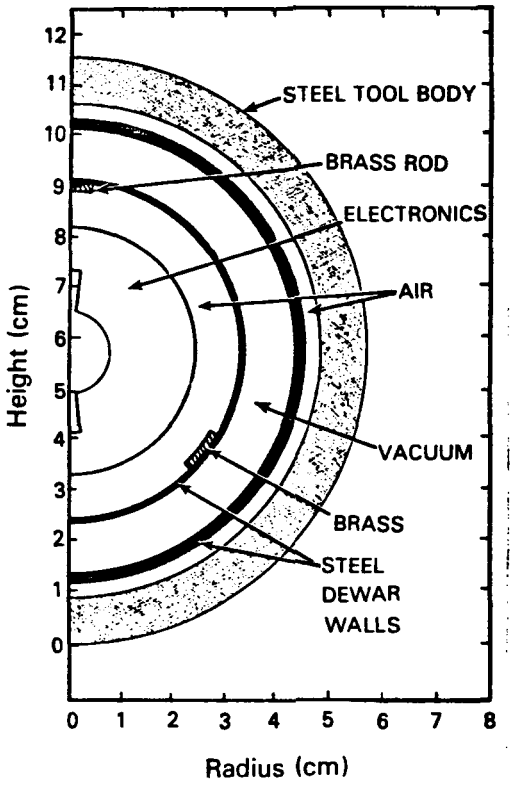

Fig. 7. Electronics section plane geometry model.

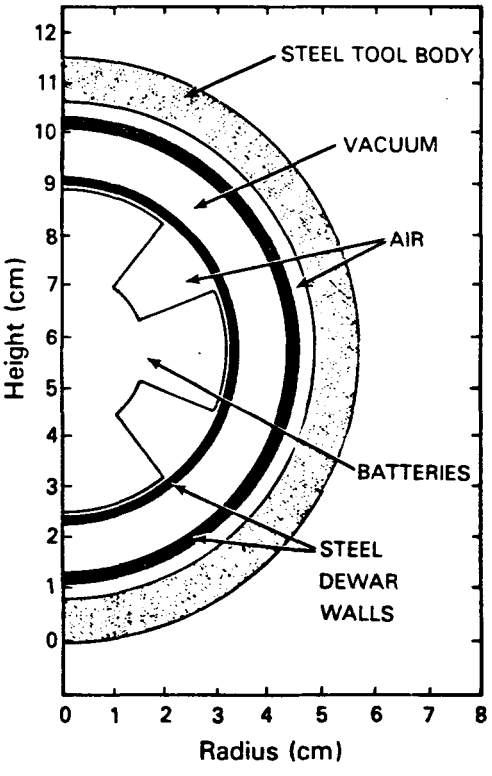

Fig. 8. Battery section plane geometry model.

temperature. The initial conditions assumed for the entire mesh are

$$T(r,z) = To = 298\ K. \quad (3)$$

The boundary condition on the outer tool body surface is based on the average trip velocity into the well and the background geothermal temperature gradient. The gradient is approximated by

$$T\infty = 300.9 + 0.06 * V * \theta. \quad (4)$$

The film coefficient on the surface is calculated using the Dittus-Boelter equation (8).

The boundary condition on the outer tool body surface varies with time and is given as the product of the film coefficient and the temperature difference across the tool body wall. At the upper end of the dewar, heat must pass through a cork plug and at the bottom heat is transferred through a 4.2-cm air gap. Solution of the partial differential equations and their associated auxiliary conditions was accomplished numerically.

RESULTS

The purpose of this investigation was to determine the input heat fluxes and the temperature field in the tool as a function of time. Figures 9, 10, and 11 show the heat flux on the outer tool surface and the temperature history.

At the given velocity, the tool reaches station at 4421 s where the temperature is 502 K (Fig. 11). The heat flux is plotted in two parts corresponding to the time interval to reach station and the time interval while parked. A curve fit was made to the flux-time results, shown in Fig. 9, using linear regression for times larger than 200 s and yielded

$$Q/A = 1350.9 + 4.696E{-}2 * \theta. \quad (5)$$

After reaching station, the input heat flux, shown in Fig. 10, drops to 6% of its previous value. This flux-time history yields a curve fit of the form

$$Q/A = 187.82EXP(-8.69E{-}5 * \theta). \quad (6)$$

The energy input per unit area for the trip into the well is 6.4 E+06 J/m². A hand calculation to estimate

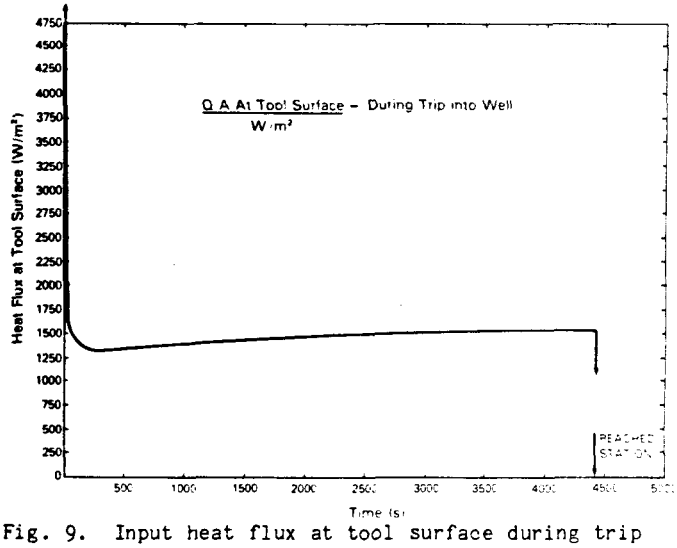

Fig. 9. Input heat flux at tool surface during trip into well.

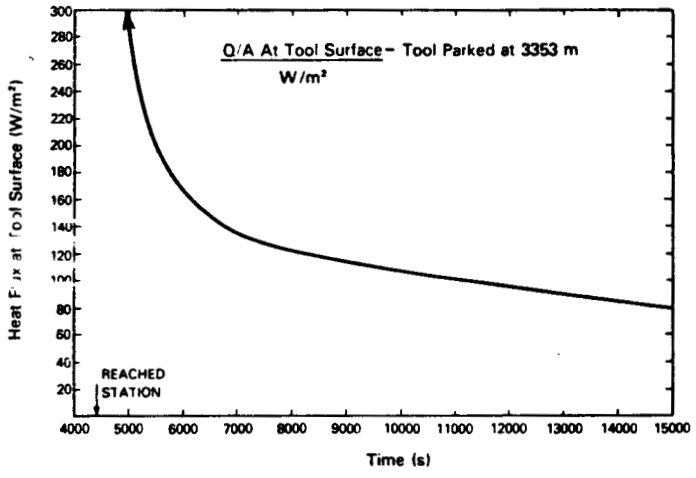

Fig. 10. Input heat flux at tool surface while parked on station.

the expected temperature change for the total mass, with equivalent specific heat and the above energy input gives ΔT = 148 K as compared to a 189 K temperature rise for the tool body. The steel tubular tool body is a major part of the thermal mass of the system, protecting the electronics for the trip into the well. The energy input per unit area while parked on station until failure is 3.37E + 6 J/m².

Figure 12 shows the plots of temperature versus radial position through the electronics section for three times during the simulation; at t=2660 s, at t=4421 s time to reach station and at t=8020 s, time approaching maximum temperature. The electronics are indeed the coolest objects in the tool. Figure 13 shows

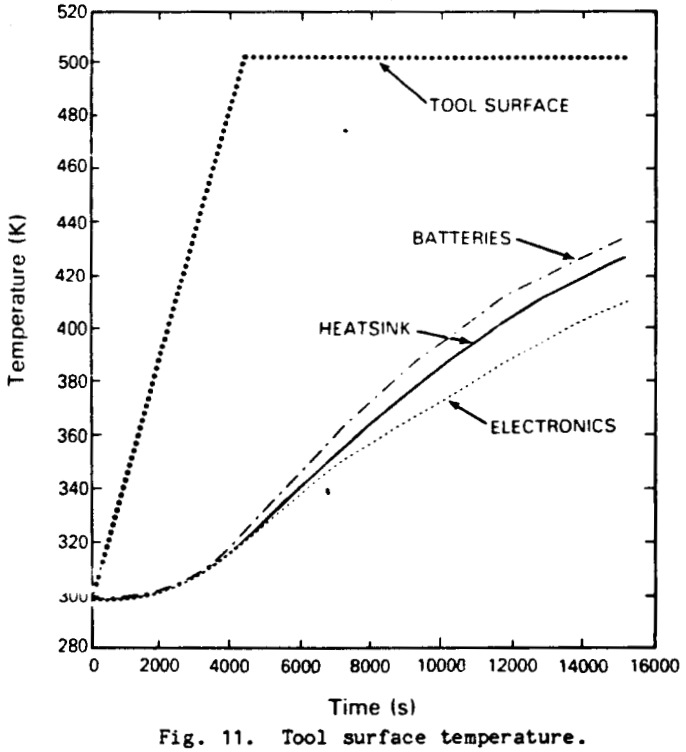

Fig. 11. Tool surface temperature.

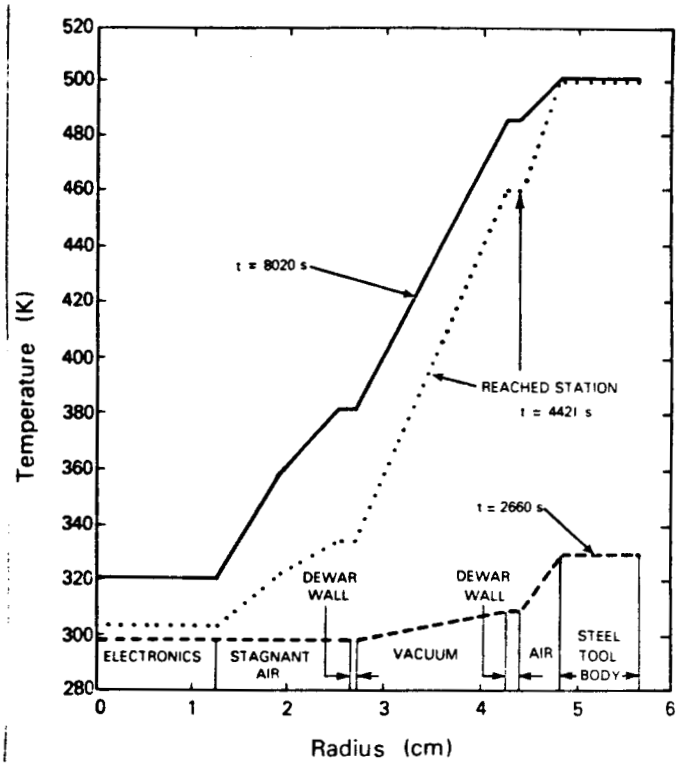

Fig. 12. Temperature vs radius at time=660 s, 4421 s, and 8020 s.

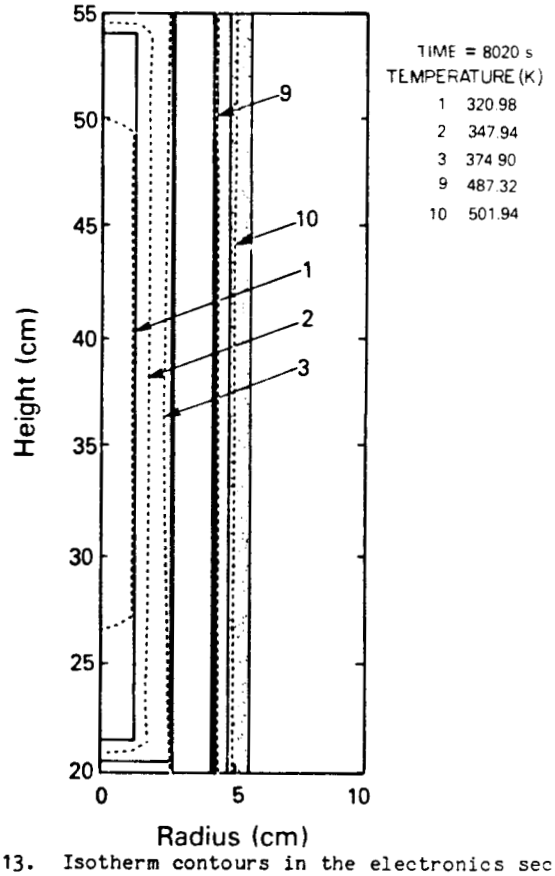

Fig. 13. Isotherm contours in the electronics section at time=8020 s.

isotherms of 348 K and 321 K in the electronics section at θ=8020 s, for bulk air and electronics respectively. Because 353 K is the maximum reliable operating temperature, the time limit is reached at approximately 8500 s, which correlates with measurements taken during the instrument development test. Assuming that the tool is removed after 8500 s at the same velocity, the air and electronics temperature rise to 368 and 348 K respectively, (Fig. 14) leaving very little margin between the calculated and maximum operating temperatures. Then, using the air temperature to determine time of retrieval is reasonable.

To investigate the thermal potentials between sections in the dewar assuming the tool remains in the well, a temperature history at each section and on the boundary is plotted in Fig. 11. At time = 8921 s, the heat sink and batteries are 48 and 57 K warmer than the electronics. The existing thermal potentials will move heat into the electronics rather than from electronics to heat sink. The available paths for heat transfer have a conductance of $4.71 \times 10^{-2} \frac{W}{m^2}$ which can transfer only 2.5 W at the given potentials. Recalling the possible explanations for the measured temperature history, both c) and d) have been shown to contribute to thermal failure.

DESIGN IMPROVEMENTS

Design improvements made to the thermal protection system involved increasing both the conductance and the thermal potential between electronics and heat sink.

Heat pipes replaced the brass rod mounting rails. For a heat pipe operating at 323 K, the conductance or axial heat flux is 4.0 E+04 W/m², which is vastly larger than the conductance of long, small diameter brass rods (11).

The thermal capacity of the heat sink is based on its volume. An increase in thermal capacity must be a result of increasing the ρc_p and $\rho^* L_{fusion}$ products of the material. Also, any materials considered must have a melting point below 353 K, the maximum electronics operating temperature. For each material considered, a calculation was made to determine the enthalpy increase of the solid, energy absorbed in melting, and enthalpy increase of the liquid between the temperature limits of 273 and 353 K. Material properties and results are listed in Table I. Tap water was chosen as the replacement heat sink material, after considering cost, availability and handling difficulties.

This choice of a heat sink material with a melting point below 353 K provides a much larger thermal potential in the right direction -- from the electronics to the heat sink. For ice, the maximum temperature difference is $\Delta T = 80^\circ$ which diminishes with time after the ice melts and the entire package heats up.

These three design changes made to the thermal protection system improved its operation by allowing energy to be absorbed as latent heat in addition to the energy already absorbed as enthalpy increases. The tool survival at given temperatures was increased by a factor of 4 and thus allowed reasonable time for making necessary measurements.

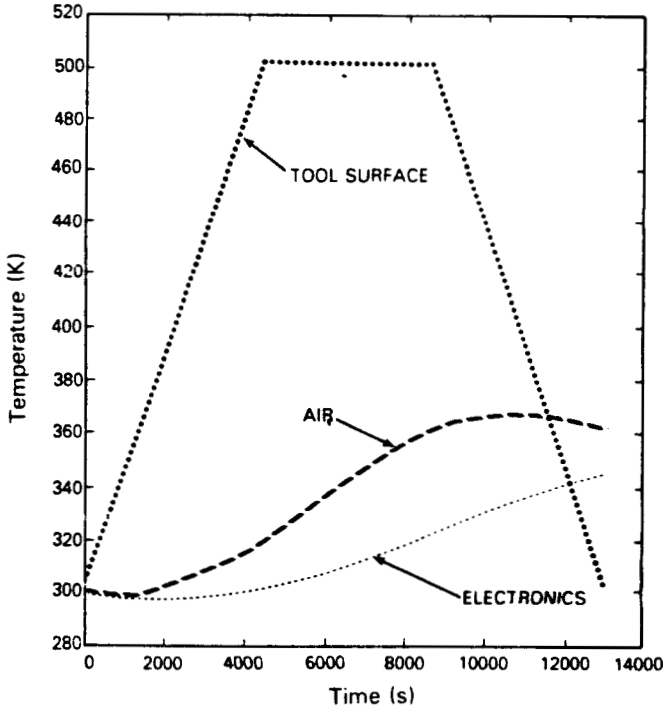

Fig. 11. Round trip temperature history for tool surface, electronics and stagnant air.

REFERENCES

1. J. C. Rowley and R. S. Carden, "Drilling of Hot Dry Rock Geothermal Energy Extraction Well EE-3," Los Alamos National Laboratory report LA-9512-HDR (August 1982).

2. R. A. Pettitt, "Planning, Drilling, Logging and Testing of Energy Extraction Hole EE-1, Phase I and II," Los Alamos Scientific Laboratory report LA-6906-MS (August 1977).

3. C. Helmick, S. Koczan, and R. Pettitt, "Planning and Drilling Geothermal Energy Extraction Hole EE-2," Los Alamos National Laboratory report LA-9302-HDR (April 1982).

4. R. G. Lawton, "The AYER Heat Conduction Computer Program," Los Alamos Scientific Laboratory report LA-5613-MS (May 1974).

5. M. J. Berger, "ZONE - A Finite Element Mesh Generator," Lawrence Livermore Laboratory report UCID-17139, Rev 1 (March 12, 1980).

6. G. A. Bennett and G. R. Sherman, "Analysis and Thermal Design Improvements of Downhole Tools for Use in Hot Dry Wells," Los Alamos National Laboratory report LA-9671-HDR (February 1983).

7. F. Kreith, Principles of Heat Transfer, (Intext Educational Publishers, New York, 1973), p 636, 126.

8. Max Jakob, Heat Transfer, (John Wiley and Sons, Inc., New York, 1949), p 547.

9. E. W. Bentilla, K. F. Starrett, and L. E. Karre, "Research and Development Study on Thermal Control By Use of Fusible Materials," Northrop Space Laboratories report NSL-65-16-1 (April 1966).

10. Metal Specialties, "Properties of Metal Specialties Alloys," Fairfield, Connecticut.

11. P. Dunn and D. A. Reay, Heat Pipes, (Pergamon Press, Oxford, 1978), p 106.

TABLE I

HEAT SINK MATERIAL

Material	Tmelt (K)	Density (kg/m^3)	Specific Heat (J/kg-K)	Latent Heat ($J/kgx10^5$)	Heat Absorbed ($Jx10^5$)
Eicosane (9) $C_{20}H_{42}$	310	788	2210	2.46	1.59
Woods Metal (10)	344	9400	167.4	0.325	2.88
Gallium (10)	303	6095	372	0.802	3.81
Ice (7)	273	913	4226	3.35	4.58